

Luminescence and EPR studies of $\text{Y}_2\text{O}_3:\text{Gd}^{3+}$ phosphors prepared via solution combustion method

Vijay Singh · R. P. S. Chakradhar ·
J. L. Rao · Isabelle Ledoux-Rak · Ho-Young Kwak

Received: 24 June 2010/Accepted: 23 August 2010/Published online: 8 September 2010
© Springer Science+Business Media, LLC 2010

Abstract Gadolinium-activated Y_2O_3 phosphor has been prepared by combustion process in a short time of 5 min. The phosphors are well characterized by X-ray diffraction, scanning electron microscopy, and energy-dispersive analysis of X-ray. The as-prepared $\text{Y}_2\text{O}_3:\text{Gd}$ powder shows that all the peaks are due to the Y_2O_3 cubic phase. Upon UV light excitation (276 nm), the phosphor exhibits a strong and sharp UV emission at 314 nm and is ascribed to $^6\text{P}_{7/2} \rightarrow ^8\text{S}_{7/2}$ transition of Gd^{3+} ions. The EPR spectrum of $\text{Y}_2\text{O}_3:\text{Gd}$ phosphor exhibits resonance signals with effective g values at $g = 1.96$, $g = 2.88$, and $g = 6.08$ and are attributed to Gd^{3+} ions located at sites with weak, intermediate, and strong cubic symmetry fields, respectively. It is observed that the population of spin levels (N) and linewidth depends on temperature. The paramagnetic susceptibility (χ) is also evaluated as a function of temperature and discussed.

Introduction

Yttrium oxide is an important material in industrial applications and is widely used due to its excellent properties such as a high dielectric constant, a low absorption in a broad range, high melting point, phase stability, low thermal expansion, high refractive index, and excellent thermal conductivity [1–4]. Y_2O_3 has a low phonon energy, which makes it a promising host material for efficient up-conversion emission [5, 6]. Y_2O_3 is one of the best hosts for Er^{3+} because of the same ionic radii of Y^{3+} and Er^{3+} [5–8]. Europium-doped Y_2O_3 is a well-known red emitting phosphor used in lightening industry and optoelectronic devices [9, 10]. For decades, yttrium oxide is also used in electronic applications as a part of metal–oxide–semiconductor (MOS) heterostructures in MOS transistors [11, 12]. The structure of the Y_2O_3 belongs to the C-type cubic bixbyite structure, space group $Ia\bar{3}$ with 16 formula units in the elementary cell. The detailed studies about the crystal structure have been reported in several publications [13–16].

Recently, the theory of electron spin relaxation of Gd^{3+} complexes and their use as probes and magnetic resonance imaging contrast agents have been widely studied [17–19]. Abdullah et al. [20] studied ultraviolet luminescence in Y_2O_3 doped with Gd ions. Enhanced luminescence intensity has been obtained from $\text{Y}_2\text{O}_3:\text{Eu}^{3+}$ thin films by the incorporation of Gd in Y_2O_3 lattice [21]. A very good substitution of dopants is ensured by similar crystal-chemical constraints for rare earth ions and yttrium. In view of this, this work has attracted many researchers [22–25]. Because of a high relaxation time, Gd^{3+} displays electron paramagnetic resonance (EPR) spectrum at room temperature [26]. EPR has proved to be a powerful tool for the characterization of local order in a variety of solid-state systems.

V. Singh (✉) · H.-Y. Kwak (✉)
Mechanical Engineering Department, Chung-Ang University,
Seoul 156-756, Korea
e-mail: vijayjiin2006@yahoo.com

H.-Y. Kwak
e-mail: kwakh@cau.ac.kr

R. P. S. Chakradhar
Glass Technology Laboratory, Central Glass and Ceramic
Research Institute, CSIR, Kolkata 700032, India

J. L. Rao
Department of Physics, Sri Venkateswara University,
Tirupati 517-502, India

I. Ledoux-Rak
Laboratoire de Photonique Quantique et Moléculaire,
Institut d'Alembert, Ecole Normale Supérieure de Cachan,
61 av. du President Wilson, 94-235 Cachan, France

In this study, we have successfully employed solution combustion process for the preparation of Gd^{3+} -activated Y_2O_3 . The structural and magnetic properties of this phosphor are well characterized by X-ray diffraction (XRD), scanning electron microscopy (SEM), energy-dispersive analysis of X-ray (EDAX) spectroscopy, EPR and photoluminescence (PL) techniques.

Experimental

In this investigation, the starting materials used for the synthesis were nitrates of Y, Gd, and Urea. The composition used in the study was $\text{Y}_{1.96}\text{Gd}_{0.04}\text{O}_3$. The doped material was prepared using 5 g $\text{Y}(\text{NO}_3)_3 \cdot 6\text{H}_2\text{O}$, 0.12 g $\text{Gd}(\text{NO}_3)_3 \cdot 6\text{H}_2\text{O}$, and 2 g $\text{CH}_4\text{N}_2\text{O}$. The metal nitrates and urea for combustion were calculated on the basis of total oxidising and reducing valences of the oxidizers and the fuel using the concepts of propellant chemistry [27]. The combustion reaction is ignited by the addition of the fuel urea. These were mixed in a China dish using minimum quantity of de-ionized water to form a solution, and later introduced into a muffle furnace maintained at 500 °C. As soon as the dish was introduced, the combustion proceeds and vapors of NO_x escape from the furnace for a few minutes. During this period, the constituents of the dish boil and form froth and finally settle into a solid, porous mass. Finally, the dish was taken out and the solid mass was crushed into a powder, which was later used for characterization.

The phase purity of $\text{Y}_2\text{O}_3:\text{Gd}$ powders was examined by using XRD (X'pert, Shimadzu, Japan) using $\text{Cu K}\alpha$ radiation ($\lambda = 0.154$ nm). The powders were taken in an adhesive tape fixed onto a stub and coated with graphite for their electron microscopic evaluation. The chemical compositions were analysed using the EDAX attached to the SEM (S-4300, Hitachi, Japan). The EPR measurements were carried out on a Bruker EMX 10/12 X-band ESR spectrometer. Excitation and emission spectra were measured at room temperature using a spectrofluorometer (JASCO, FP-6500, Japan) equipped with a Xe source.

Results and discussion

X-ray diffraction

Figure 1 shows the X-ray diffraction pattern of as-prepared $\text{Y}_2\text{O}_3:\text{Gd}$ phosphor powder. The observed pattern is found to match with the standard JCPDS files (83-0927). Calculated cell parameters are in very good agreement with the literature data [28] and JCPDS files (83-0927). Therefore, all the peaks are due to the Y_2O_3 cubic phase and no

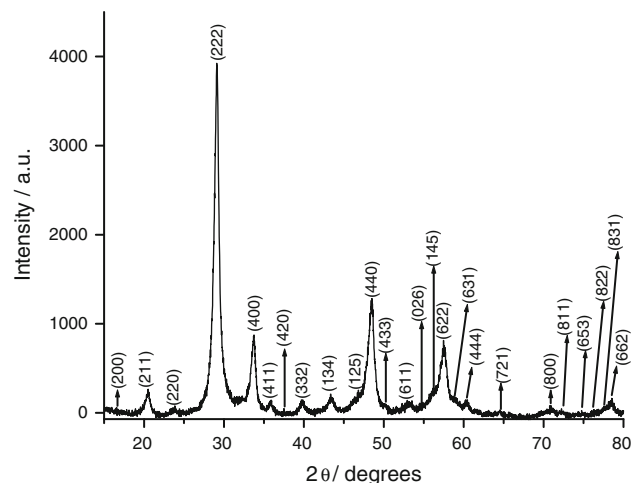


Fig. 1 Powder XRD pattern of $\text{Y}_2\text{O}_3:\text{Gd}^{3+}$ phosphor

impurity crystalline phases can be detected. These results show that the formation of Y_2O_3 phase could be formed even at furnace temperatures as low as 500 °C, which is several hundred degrees lower than the conventional solid-state reaction.

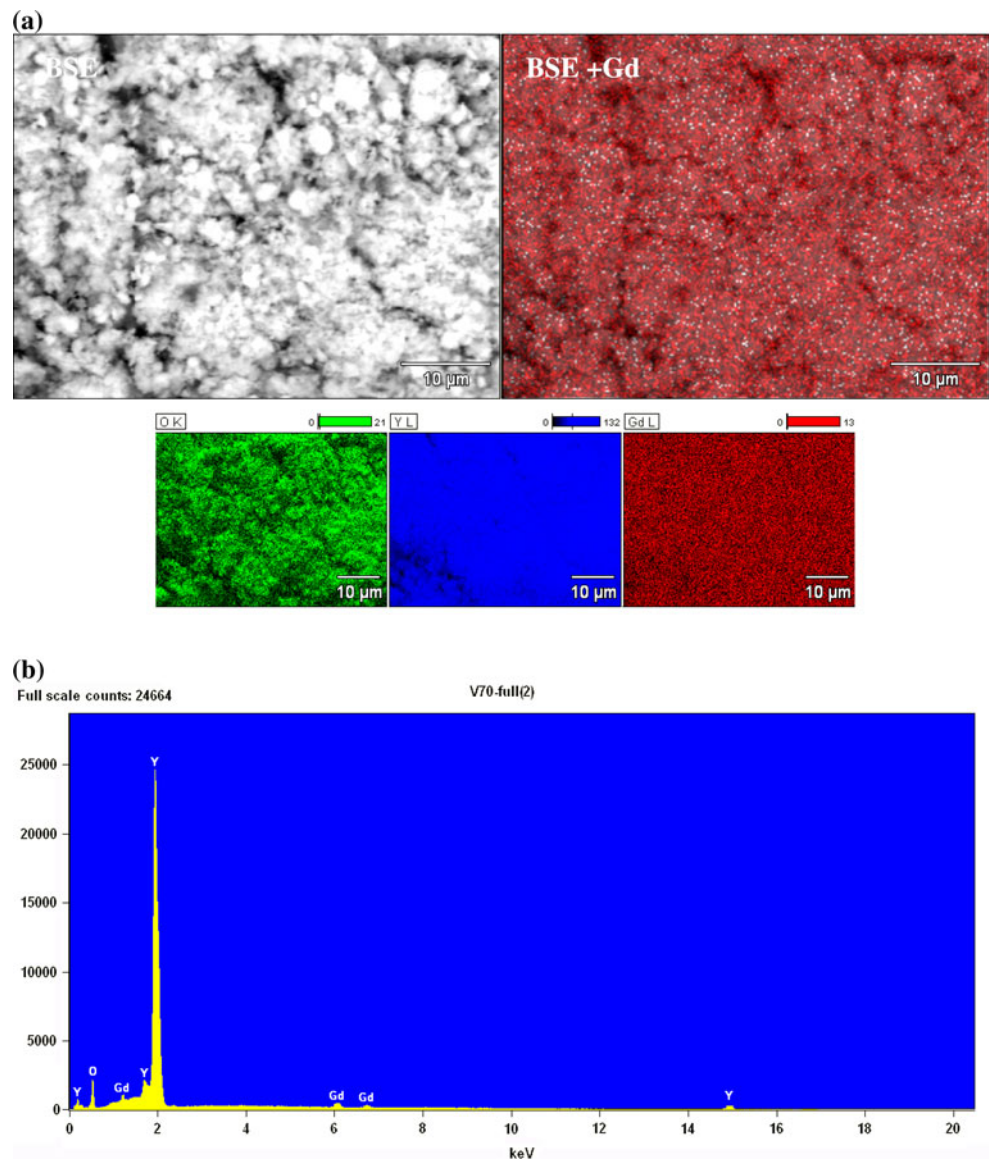
Scanning electron microscopy and energy-dispersive analysis of X-ray spectroscopy study

The morphological study along with chemical composition determination was done using SEM coupled with EDAX. Figure 2a represents the SEM micrograph of combustion synthesized $\text{Y}_2\text{O}_3:\text{Gd}$ powder taken using backscattered electron (BSE) detection mode to understand their morphology. The figure suggests that the particles are agglomerated. Figure 2a shows the elemental mapping for Y, O, and Gd, which indicates homogeneous distribution of each element. Further, in order to know the distribution of Gd, the overlapping of BSE and EDAX mapping for Gd is shown (Fig. 2a, BSE + Gd). It is clear from this micrograph that gadolinium ions have been doped into Y_2O_3 matrix homogeneously. Figure 2b shows the EDAX spectrum which also indicates that the as-obtained product is composed of Y, O, and Gd. The peaks corresponding to Gd indicate its presence even with very low doping concentration.

Electron paramagnetic resonance studies

Figure 3a, b shows the EPR spectrum of $\text{Y}_2\text{O}_3:\text{Gd}$ powder at room temperature and at 110 K, respectively. The EPR spectra exhibit three prominent signals with effective g values at $g = 6.08$, 2.88, and 1.96. This observed spectrum has been labeled as the U-spectrum [29–32] and is the most frequent signature of S-state rare-earth ion in a low symmetry site. The EPR spectral features of Gd^{3+} ions

Fig. 2 **a** Backscattered electron (BSE) SEM and EDAX mapping of Y, O, Gd, and **b** EDAX spectrum



depend on the relative magnitude of Zeeman microwave frequency and crystal field strength. When the microwave frequency is smaller compared to the crystal field strength, the resonance lines of Gd^{3+} can be seen in the range $g > 2$. When the microwave frequency is of the same order to that of the crystal field strength, the zero-field resonance can be seen. If the microwave frequency is larger than the crystal field strength the resonance signals will be concentrated in the vicinity of $g = 2.0$.

Chepeleva et al. [29] were the first to discuss the U-spectrum, and they attributed the $g = 6.0$ resonance to a strong cubic field on the basis of solutions obtained for a cubic Hamiltonian in the strong crystal field limit, where the Zeeman interaction may be treated as a perturbation. Another early but more detailed analysis of the U-spectrum was performed by Niklin et al. [30]. They searched

extensively for a single set of rhombic crystal field parameters that could simultaneously account for all the principal features of the U-spectrum, but they attributed the three prominent features to three distinct types of crystal fields. The $g = 6.0$ feature was attributed to a strong cubic crystal field, as in the interpretation given by Chepeleva et al. [29]. Cugunov and Kliava [32] and Koopmans et al. [33] employed computer simulation techniques in their analysis but their final interpretations differ from each other. Cugunov and Kliava [32] attributed the $g = 6.0$ to a well-defined rhombic crystal field and the broad resonance encompassing $g = 2.0$ is due to the formation of Gd^{3+} clusters. In contrast, the $g = 6.0$ resonance was considered to be a feature characteristic of intermediate crystal field sites of axial symmetry and has attributed the broadened general appearance of the U-spectrum to isolated rare earth

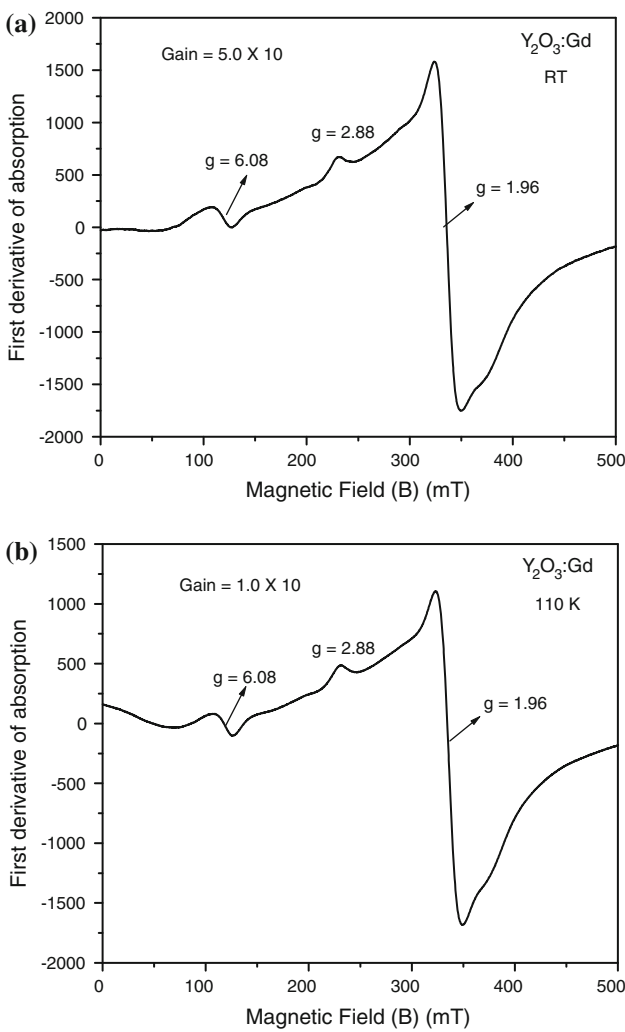


Fig. 3 EPR spectrum of $\text{Y}_2\text{O}_3:\text{Gd}^{3+}$ phosphor at **a** room temperature and **b** at 110 K

ions in wide varieties of sites. The EPR signals observed in the present study with effective g values at $g = 1.96$, 2.88, and 6.08 are due to Gd^{3+} ions located at sites with weak, intermediate and strong cubic symmetry fields, respectively. The zero-field splitting parameter (D) can be estimated based on the ΔB values (between the central line and the edge line of the lower magnetic field in the EPR spectrum) using the formula $D \approx \Delta B/6$ which is valid for the first order of the perturbation theory [34]. The estimated D value is found to be 36.23 mT which is of the same order reported for Gd^{3+} ions in various complexes [34–36].

The population of spin levels participating in resonance can be calculated by comparing the area under the absorption curve with that of a standard ($\text{CuSO}_4 \cdot 5\text{H}_2\text{O}$ in this study) of known concentration. Weil et al. [37] gave the following expression which includes the experimental parameters of both the sample and the standard:

$$N = \frac{A_x(\text{scan}_x)^2 G_{\text{std}}(B_m)_{\text{std}}(g_{\text{std}})^2 [S(S+1)]_{\text{std}}(P_{\text{std}})^{1/2}}{A_{\text{std}}(\text{scan}_{\text{std}})^2 G_x(B_m)_x(g_x)^2 [S(S+1)]_x(P_x)^{1/2}} [\text{std}] \quad (1)$$

where A is the area under the absorption curve, which can be obtained by double integrating the first derivative EPR absorption curve, scan is the magnetic field corresponding to a unit length of the chart, G is the gain, B_m is the modulation field width, g is the g factor, S is the spin of the system in its ground state. P is the power of the microwave source. The subscripts “ x ” and “ std ” represent the corresponding quantities for the $\text{Y}_2\text{O}_3:\text{Gd}$ powder and the reference ($\text{CuSO}_4 \cdot 5\text{H}_2\text{O}$), respectively. It is observed that as the temperature is lowered from room temperature to 110 K the spin population for the $g = 1.96$ increases from 0.63×10^{20} to 9.41×10^{20} obeying the Boltzmann law. Further it has also been observed that the linewidth of the $g = 1.96$ resonance is increased slightly from 25.2 to 26.0 mT. The increase in linewidth is due to spin–spin interaction between the $\text{Gd}–\text{Gd}$ ions. An increase of spin–spin interaction with the decrease of temperature results in broadening of resonance line.

The EPR data can be used to calculate the paramagnetic susceptibility of the sample using the formula [38]

$$\chi = \frac{Ng^2\beta^2J(J+1)}{3k_B T} \quad (2)$$

where N is the number of spins/ m^3 and the other symbols have their usual meaning. N can be calculated from Eq. 1 and g is taken from EPR data. Since the resonance signal at $g = 1.96$ is intense, this g value is used in calculating the paramagnetic susceptibility. The paramagnetic susceptibility (χ) evaluated from EPR data at room temperature and at 110 K are found to be $0.15 \times 10^{-4} \text{ kg m}^{-3}$ and $2.2 \times 10^{-4} \text{ kg m}^{-3}$, respectively. The main advantage of calculating susceptibility from EPR data is that the diamagnetic contribution can be neglected.

Photoluminescence studies

Figure 4a shows the excitation spectrum of $\text{Y}_2\text{O}_3:\text{Gd}^{3+}$ observed at room temperature. The spectrum exhibits an intense band at 276 nm (36230 cm^{-1}) with several weak bands on the higher energy side. These bands can be ascribed to the Gd^{3+} , 4f–4f intra configurational transitions between ${}^8\text{S}$ ground state and ${}^6\text{I}_J$ and ${}^6\text{D}_J$ multiplets [39]. The observed band positions and their assignments are given in Table 1. The observed band positions are in good agreement with the optical absorption band positions reported for Gd^{3+} ions by Binnemans et al. [40].

Figure 4b shows the emission spectrum observed in the ultra violet region with excitation wavelength fixed at

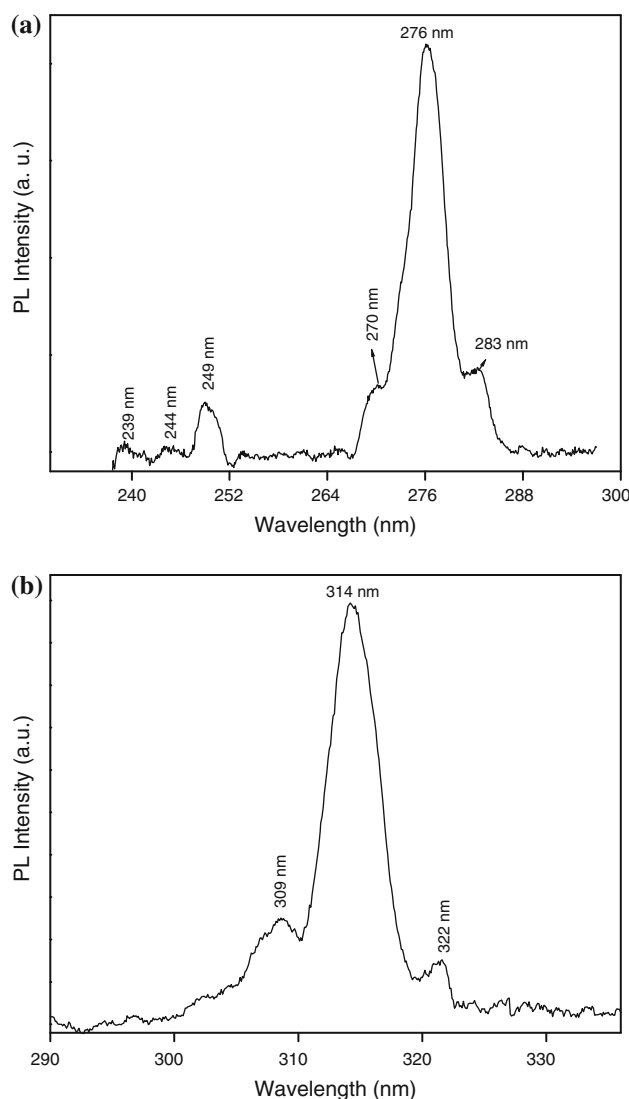


Fig. 4 Photoluminescence spectra of the Y₂O₃:Gd³⁺ phosphor
a Excitation spectrum of Y₂O₃:Gd³⁺ ($\lambda_{\text{em}} = 314 \text{ nm}$) and b Emission spectrum of Y₂O₃:Gd³⁺ ($\lambda_{\text{ex}} = 276 \text{ nm}$)

Table 1 The observed band positions for Y₂O₃:Gd³⁺ along with their assignments

Transition from $^8S_{7/2}$ to	Observed band positions	
	Wavelength (nm)	Wavenumber (cm ⁻¹)
$^6I_{7/2}$	283	35335
$^6I_{9/2}$, $^6I_{11/2}$	276	36230
$^6I_{13/2}$	270	37040
$^6D_{9/2}$	249	40160
$^6D_{7/2}$	244	40980
$^6D_{3/2}$, $^6D_{5/2}$	239	41840

276 nm. The emission spectrum exhibits an intense band centered at 314 nm (31847 cm⁻¹) and two weak bands on either side of the intense band. Abdullah et al. [20]

observed a similar spectrum band for Gd³⁺-doped Y₂O₃ prepared by heating of precursors in a polymer solution.

Gd³⁺ is unique among triply ionized rare-earth ions having an energy difference between the $^8S_{7/2}$ ground state and the first excited state $^6P_{7/2}$ which is the largest in the series. According to the mean free-ion parameters of Gd³⁺, the excited state is predicted to be $\sim 32,200 \text{ cm}^{-1}$, above the ground state [41]. The intense peak observed at 314 nm (31850 cm⁻¹) has been attributed to $^6P_{7/2} \rightarrow ^8S_{7/2}$ of Gd³⁺ ions. A weak photoluminescence band observed at 309 nm (32360 cm⁻¹) has been assigned to $^6P_{5/2} \rightarrow ^8S_{7/2}$ transition. Vetter et al. [42] and Shishonok et al. [41] observed a similar peak for Gd³⁺ ion in AlN and BN, respectively. Moreover, Shishonok et al. [41] observed an energy difference between $^6P_{7/2}$ and $^6P_{5/2}$ is equal to $\sim 77 \text{ meV}$ ($\sim 620 \text{ cm}^{-1}$). In this work, the authors observed energy difference between $^6P_{7/2}$ and $^6P_{5/2}$ is equal to 520 cm⁻¹ which confirms the assignment of the transition for the weak emission band observed at 309 nm. The emission band observed at 322 nm (=31055 cm⁻¹) may be due to some impurity from the host. As the ionic radii of Y³⁺ (1.04 Å⁰) and Gd³⁺ (1.08 Å⁰) are comparable, it is reasonable to assume that Gd³⁺ ions occupy Y³⁺ ion sites [43] in this phosphor.

Conclusions

We could synthesize the Gd-doped Y₂O₃ powder via combustion process. The major advantages of the combustion process are its simple, speed energy saving, cost effectiveness, homogeneity, and purity. This method is able to produce single phase Y₂O₃ directly. By EDAX analysis, it is observed that Y₂O₃ was found to be pure and displays a homogeneous Gd distribution. The EPR spectrum exhibits resonance signals at $g = 1.96$, 2.88, and 6.08 which are attributed to Gd³⁺ ions located at sites with weak, intermediate, and strong cubic symmetry fields, respectively. The feature at $g = 1.96$ indicates the existence of small crystal field splittings compared with the X-band quantum. As the temperature is lowered from room temperature to 110 K the spin population for the resonance signal at $g = 1.96$ increases significantly following the Boltzmann law. At 110 K, an increase in linewidth is observed for the resonance signal at $g = 1.96$ which has been attributed to spin–spin interaction. The excitation spectrum exhibits several bands characteristic of Gd³⁺ ions. The emission spectrum exhibits a strong and sharp band in the UV region and is ascribed to $^6P_{7/2} \rightarrow ^8S_{7/2}$ transition of Gd³⁺ ions.

Acknowledgements Dr. Vijay Singh expresses his thanks to the Chung-Ang University, Seoul (South Korea) for providing the Research Assistant Professorship. Dr. R. P. S. Chakradhar is grateful

to Dr. H. S. Maiti, Director, CGCRI and Dr. K. K. Phani, Head, GTL lab, CGCRI for their constant support and encouragement.

References

1. Kaminskii KK (1990) *Laser Crystals*. Springer, Berlin
2. Fornasiero L, Mix E, Peters V, Peterman K, Huber G (2002) *Ceram Int* 26:589
3. Senatsky Y, Shirakawa A, Sato Y, Hagiwara J, Lu J, Ueda K, Yagi H, Yanagitani T (2004) *Laser Phys Lett* 1:500
4. Kong J, Tang DY, Lu J, Ueda K, Yagi H, Yanagitani T (2004) *Opt Lett* 29:1212
5. Zhang J, Wang S, An L, Liu M, Chen L (2007) *J Lumin* 122–128:8
6. Matsuura D, Ikeuchi T, Soga K (2008) *J Lumin* 128:1267
7. Li X, Li Q, Wang J, Li J (2007) *J Lumin* 124:351
8. Eilers H (2009) *J Alloys Compd* 474:569
9. Jung KY, Kang YC, Park YK (2008) *J Ind Eng Chem* 14:224
10. Shionoya S, Yen WM (1999) *Phosphors Handbook*. CRC Press, New York
11. Gaboriaud RJ, Pailloux F, Guerin P, Paumier F (2001) *Thin Solid Films* 400:106
12. Zhang S, Xiao R (1998) *J Appl Phys* 83:3842
13. Yakel HL (1979) *Acta Crystallogr B* 35:564
14. Hanic F, Hartmova M, Knab GG, Uruskovkaya AA, Bagdasarov KS (1984) *Acta Crystallogr B* 40:76
15. Silver J, Martinez-Rubio MI, Ireland TG, Withnall R (2001) *J Phys Chem B* 105:7200
16. Klintenberg M, Edvardsson S, Thomas JO (1998) *J Alloys Compd* 275–277:174
17. Lei XG, Jockusch S, Turro NJ, Tomalia DA, Ottaviani MF (2008) *J Colloid Interface Sci* 322:457
18. Zhou X, Westlund P-O (2005) *J Magn Reson* 173:75
19. Benmelouka M, van Tol J, Borel A, Port M, Helm L, Brunel LC, Merbach AE (2006) *J Am Chem Soc* 128:7807
20. Abdullah M, Khairurrijal, Waris A, Sutrisno W, Nurhasanah I, Vioktalamo AS (2008) *Powder Technol* 183:297
21. Bae JS, Jeong JH, Shim KS, Kim SB, Moon BK, Yi SS (2005) *Thin Solid Films* 476:35
22. Lagutin AS, Fedorov GE, Kopylov AV, Vanacken J, Herlach F (1998) *Physica B* 246–247:520
23. Shen Z, Nygren M (1997) *J Eur Ceram Soc* 17:1639
24. Chen G, Takenoshita H, Kamegashira N (1996) *Mater Chem Phys* 46:43
25. Pureur P, Creuzet G, Fert A (1985) *J Magn Magn Mater* 53:121
26. Bunzli JCG, Choppin GR (1989) Lanthanides probes in life, chemical and earth sciences, Chapters 4, 6, and 7. Elsevier, Amsterdam
27. Kingsley JJ, Patil KC (1988) *Mater Lett* 6:427
28. Allieri B, Depero LE, Marino A, Sangaletti L, Caporaso L, Speghini A, Bettinelli M (2000) *Mater Chem Phys* 66:164
29. Chepeleva IV, Lazukin VN, Demdovskii SA (1967) *Sov Phys Dokl* 11:864
30. Nicklin RC, Johnstone JK, Barnes RG, Wilder DR (1973) *J Chem Phys* 59:1652
31. Iton LE, Turkevich J (1977) *J Phys Chem* 81:435
32. Cugunov L, Kliava J (1982) *J Phys C15:L933*
33. Koopmans HJA, Peric MM, Niuzenhuijse B, Gallings PJ (1993) *Phys Status Solidi (b)* 120:745
34. Szyczewski A, Lis S, Kruczynski Z, But S (2002) *J Alloys Compd* 341:307
35. Brodbeck CM, Iton LE (1985) *J Chem Phys* 83:4285
36. Geeta G, Jaganathan R (1989) *Spectrochim Acta* 45A:829
37. Weil JA, Bolton JR, Wertz JE (1994) Electron paramagnetic resonance-elementary theory and practical applications. Wiley, New York, p 498
38. Aschcroft NW, Mermin ND (2001) “Solid State Physics”. Harcourt College Publishers, San Diego, p 656
39. Moretti F, Chioldini N, Fasoli M, Griguta L, Vedda A (2007) *J Lumin* 126:759
40. Binnemans K, Gorller-Walrand C, Adam JL (1997) *Chem Phys Lett* 280:333
41. Shishonok EM, Leonchik SV, Steeds JW, Wolverson D (2007) *Diam Relat Mater* 16:1602
42. Vetter U, Zenneck J, Hofmann H (2003) *Appl Phys Lett* 83:2145
43. Simon S, Eniu D (2007) *J Mater Sci* 42:5949. doi:[10.1007/s10853-007-1717-4](https://doi.org/10.1007/s10853-007-1717-4)